

Neuregulin-1 promotes functional improvement by enhancing collateral sprouting in SOD1^{G93A} ALS mice and after partial muscle denervation

Renzo Mancuso^{1,6*}, Anna Martínez-Muriana^{1*}, Tatiana Leiva¹, David Gregorio², Lorena Ariza², Marta Morell¹, Jesús Esteban-Pérez³, Alberto García-Redondo³, Ana C. Calvo⁴, Gabriela Atencia-Cebreiro³, Gabriel Corfas⁴, Rosario Osta⁵, Assumpció Bosch², Xavier Navarro¹

¹ Institute of Neurosciences and Department of Cell Biology, Physiology and Immunology, Universitat Autònoma de Barcelona, and Centro de Investigación Biomédica en Red sobre Enfermedades Neurodegenerativas (CIBERNED), Bellaterra, Spain.

² Center of Animal Biotechnology and Gene Therapy and Department of Biochemistry and Molecular Biology, Universitat Autònoma de Barcelona, Bellaterra, Spain.

³ Unidad de ELA, Servicio de Neurología, Instituto de Investigación Biomédica. Hospital 12 de Octubre “i+12”, Madrid, Spain, and Centro de Investigación Biomédica en Red de Enfermedades Raras (CIBERER), Valencia, Spain.

⁴ Department of Otolaryngology – Head and Neck Surgery, Kresgae Hearing Research Institute, University of Michigan, Michigan, US.

⁵ Laboratorio de Genética y Bioquímica (LAGENBIO), Facultad de Veterinaria, Instituto Agroalimentario de Aragón (IA2), Instituto de Investigación Sanitaria Aragón, Universidad de Zaragoza, Zaragoza, Spain

⁶ Center for Biological Sciences, University of Southampton, Southampton General Hospital, Southampton, UK.

* Both authors equally contributed as first author to the work.

Corresponding author: Dr. Xavier Navarro, Unitat de Fisiologia Mèdica, Facultat de Medicina, Universitat Autònoma de Barcelona, E-08193 Bellaterra, Spain. E-mail: xavier.navarro@uab.cat

© <2016>. This manuscript version is made available under the CC-BY-NC-ND 4.0 license

<http://creativecommons.org/licenses/by-nc-nd/4.0/>

This is a non-final version of an article published in final form in

Neurobiology of Disease 2016, 95:168–178. doi: [10.1016/j.nbd.2016.07.023](https://doi.org/10.1016/j.nbd.2016.07.023).

Abstract

Amyotrophic lateral sclerosis (ALS) is a neurodegenerative disease characterized by progressive degeneration of motoneurons, which is preceded by loss of neuromuscular connections in a “dying back” process. Neuregulin-1 (Nrg1) is a neurotrophic factor essential for the development and maintenance of neuromuscular junctions, and Nrg1 receptor ErbB4 loss-of-function mutations have been reported as causative for ALS. Our main goal was to investigate the role of Nrg1 type I (Nrg1-I) in SOD1^{G93A} mice muscles. We overexpressed Nrg1-I by means of an adeno-associated viral (AAV) vector, and investigated its effect by means of neurophysiological techniques assessing neuromuscular function, as well as molecular approaches (RT-PCR, western blot, immunohistochemistry, ELISA) to determine the mechanisms underlying Nrg1-I action. AAV-Nrg1-I intramuscular administration promoted motor axon collateral sprouting by acting on terminal Schwann cells, preventing denervation of the injected muscles through Akt and ERK1/2 pathways. We further used a model of muscle partial denervation by transecting the L4 spinal nerve. AAV-Nrg1-I intramuscular injection enhanced muscle reinnervation by collateral sprouting, whereas administration of lapatinib (ErbB receptor inhibitor) completely blocked it. We demonstrated that Nrg1-I plays a crucial role in the collateral reinnervation process, opening a new window for developing novel ALS therapies for functional recovery rather than preservation.

Keywords: neuregulin-1, amyotrophic lateral sclerosis, neuromuscular junction, motoneuron, collateral sprouting.

Introduction

ALS is a progressive degenerative disease selectively affecting motoneurons (Kiernan et al., 2011). Approximately 10% of patients have familial forms, caused by mutations in a variety of genes, the most prevalent involving the *superoxide dismutase 1 (sod1)* gene and hexanucleotide repeat expansions in *chromosome-9 open reading frame 72 (C9ORF72)* (Andersen and Al-Chalabi, 2011; Turner et al., 2013). Although *C9ORF72* gene mutations are reported in a higher proportion of ALS and ALS-frontotemporal lobar degeneration patients (DeJesus-Hernandez et al., 2011; Renton et al., 2011), SOD1-based models are still the most used tool for basic and preclinical studies. The most widely used ALS model is a transgenic mouse over-expressing the human mutated form of the SOD1 gene with a glycine to alanine conversion at the 93rd amino acid (Gurney et al., 1994; Ripps et al., 1995), which recapitulates the most relevant clinical and histopathological features of both familial and sporadic ALS (Ripps et al., 1995; Mancuso et al., 2011a; 2011b). High copy SOD1^{G93A} transgenic mice develop rapidly progressive motoneuron loss, with locomotor deficits from 12-13 weeks of age, hindlimb weakness and muscle atrophy, culminating in paralysis and death between ages 16 and 19 weeks (Ripps et al., 1995; Mancuso et al., 2011a; 2011b). Alterations in SOD1 protein have also been found in sporadic ALS patients (Bosco et al., 2010), and accumulation of wild-type SOD1 was reported to produce ALS in mice (Graffmo et al., 2013).

The death of motoneurons in ALS is preceded by failure of neuromuscular junctions (NMJs) and axonal retraction (Azzouz et al., 1997; Fischer et al., 2004; Mancuso et al., 2011b; Fischer et al., 2012), which seem dependent upon the interaction of motor axons with accompanying terminal Schwann cells and skeletal muscle fibers. Axonal sprouting is a natural mechanism attempting to compensate muscle denervation in motoneuron diseases and after nerve trauma (Tam and Gordon, 2003a). Intact motoneurons expand the size of their motor units to reinnervate denervated endplates within the same muscle, enabling to compensate for the loss of functional motor units and recover muscle strength. Motor unit enlargement by axonal sprouting is restricted even under normal conditions to a limit of 3–5 fold, thus compensating for loss of up to 85% of the total muscle function (Trojan et al., 1991; Tam and Gordon, 2003b). Although collateral sprouting has been described to occur during ALS disease process (Frey et al., 2000), it is reduced compared to normal and does not achieve enough sustained functional compensation (Shefner et al., 2006; Mancuso et al., 2011b).

Neuregulin-1 (Nrg1) is a neurotrophic factor essential for normal development, as well as for maintaining normal function in the mature nervous system (Esper et al., 2006; Stassart et al., 2012). Nrg1 contributes to axonal regeneration and normal myelination in mice (Stassart et al.,

2012) through its effects on Schwann cells, whereas silencing of Nrg1 impairs axonal regeneration (Fricker et al., 2011). It also plays an important role in NMJ maintenance (Wolpowitz et al., 2000) by regulating multiple aspects of Schwann cell differentiation, proliferation, motility, and myelination (Esper et al., 2006) and promoting acetylcholine receptor clustering at the NMJ during development (Ngo et al., 2012). Nrg1 increases terminal Schwann cells survival after postnatal denervation and promotes process extension required for new NMJ formation (Trachtenberg and Thompson, 1996; Hayworth et al., 2006). It has been also shown that Nrg1 alterations produce severe deficits in the formation and maturation of muscle spindles, thereby compromising the proprioceptive sensory system (Cheret et al., 2013). The exact role of Nrg1 type I (hereafter named Nrg1-I) on the peripheral nervous system is not fully known. It has been reported that Nrg1-I expression by Schwann cells is essential for promoting axonal regeneration and remyelination (Stassart et al., 2012). In addition, Nrg1-I administration has been shown to alleviate Charcot-Marie-Tooth disease in mice (Fledrich et al., 2014). Nrg-1/ErbB system alterations have been related to ALS, with reduced Nrg1 type-III expression in ALS patients and SOD1^{G93A} mice (Song et al., 2012). Loss-of-function mutations on Nrg1 receptor ErbB4 produce late-onset ALS in human patients (Takahashi et al., 2013). Because the manipulation of Nrg1 expression might represent a promising novel approach to treat ALS, the main goals of the present work were to investigate the contribution of the extracellular domain of Nrg1-I in ALS and to test the effect of its overexpression at the NMJs in SOD1^{G93A} ALS mice.

Material and methods

Transgenic mice

SOD1^{G93A} transgenic mice (B6SJL-Tg[SOD1-G93A]1Gur) were obtained from the Jackson Laboratory (Bar Harbor, ME, USA). Hemizygotes B6SJL SOD1^{G93A} males were obtained by crossing with B6SJL females from the CBATEG (Bellaterra, Spain). The offspring was identified by PCR of DNA extracted from tail tissue. Mice were kept in standard conditions of temperature (22±2 °C) and a 12:12 light:dark cycle with access to food and water *ad libitum*. All experimental procedures were approved by the Ethics Committee of the Universitat Autònoma de Barcelona, where the animal experiments were performed. The following experimental groups of SOD1^{G93A} mice were used in this study: SOD1+AAV-Nrg1-I (n=20, 10 per each sex), SOD1+AAV-GFP (n=10, 5 per each sex), SOD1 untreated (n=10, 5 per each sex), wild type littermates+AAV-Nrg1-I (n=10) and untreated wild type littermates (n=10). For partial denervation studies, wild type mice were distributed in three groups: rhizotomy+vehicle (n=10), rhizotomy+AAV-Nrg1-I (n=9), rhizotomy+lapatinib (n=9). To compensate the experimental groups, we divided the animals according to their weight, the results of pre-treatment electrophysiological tests and, in the case of SOD1^{G93A} mice, also the litter of origin. All experiments were performed by blinded researchers.

Virus production and injection

The cDNA sequence of the extracellular domain of Nrg1-I isoform containing a HA-tag was kindly provided by G. Corfas (Harvard Medical School, Boston, MA) and cloned between AAV2 ITRs under the regulation of the CMV promoter. The woodchuck hepatitis virus responsive element (WPRE) was added at 3' to stabilize mRNA expression. AAV1 viral stocks were produced by the Viral Production Unit of UAB (<http://sct.uab.cat/upv>) as previously described (Trachtenberg and Thompson, 1996) by triple transfection into HEK293-AAV cells of the expression plasmid, Rep1Cap2 plasmid containing AAV genes (kindly provided by J.M. Wilson, University of Pennsylvania, Philadelphia, USA) and pXX6 plasmid containing adenoviral genes (Hayworth et al., 2006) needed as helper virus. AAV particles were purified by iodixanol gradient. Titration was evaluated by picogreen (Invitrogen) quantification and calculated as viral genomes per milliliter (vg/ml). Control serotype-matching AAV1 vectors coding mock or GFP were used as control.

For intramuscular administration, 1x10¹¹ vg of AAV1-Nrg1-I in a total volume of 20 μ l were injected in the gastrocnemius muscles bilaterally using a 33G needle connected to a Hamilton syringe in isoflurane-anesthetized mice. AAV1-GFP virus was used as control.

Partial denervation of hindlimb muscles

Surgeries were performed in 5 months-old female B6SJL mice under anesthesia with ketamine (100 mg/ml) and xylazine (10 mg/ml). A small incision was made in the skin of the dorsum above the iliac crest to expose the spinal nerves on the right side. Using fine forceps and microscissors, the vertebrae were cleared of muscle, a small laminectomy was performed to expose L4 spinal root, and the root was cut at postganglionic level. The incision was sutured and the mice allowed recovering before being returned to their cages. For the next 15 days, all experimental mice were subject to daily checks for assessment of health and mobility.

Drug administration

Lapatinib ditosylate (lapatinib, Eurodiagnostico) was used to block tyrosine kinase activity of ErbB receptors. 50 μg of the drug were injected in the gastrocnemius muscles of the animals immediately after the surgery, and daily intraperitoneal injections (50 mg/kg) were given from day 1 post injury until the end of the follow up.

Electrophysiological tests

For motor nerve conduction tests the sciatic nerve was stimulated percutaneously by means of single pulses of 20 μs duration (Grass S88) delivered through a pair of needle electrodes placed at the sciatic notch. The compound muscle action potential (CMAP, M wave) was recorded from tibialis anterior, gastrocnemius and plantar interossei muscles with microneedle electrodes (Navarro and Udina, 2009; Mancuso et al., 2011b). All potentials were amplified and displayed on a digital oscilloscope (Tektronix 450S) and the amplitude from baseline to the maximal negative peak were measured. Mice body temperature was kept constant by means of a thermostated heating pad.

Motor unit number estimation (MUNE) was made using the incremental technique (Shefner et al., 2006; Lago et al., 2007; Mancuso et al., 2011b) with the same setting as for motor nerve conduction tests. Starting from subthreshold intensity, the sciatic nerve was stimulated with single pulses of gradually increasing intensity and quantal increases in the CMAP were recorded. Increments $>50 \mu\text{V}$ were considered as the recruitment of an additional motor unit. The mean amplitude of a single motor unit was calculated as the average of 15 consistent increases. The estimated number of motor units results from the equation: $\text{MUNE} = \text{CMAP maximal amplitude} / \text{mean amplitude of single motor unit action potentials}$.

Histology

Mice were transcardially perfused with 4% paraformaldehyde in PBS and the lumbar spinal cord, tibial nerve and gastrocnemius muscles were harvested. For spinal motoneuron evaluation, spinal cords were postfixed during 4h, cryopreserved in 30% sucrose in PBS, and 40 μm transverse sections cut using a cryotome (Leica) and collected serially in Olmos solution (100mM phosphate buffer pH 7.2, 30% sucrose, 1% polyvinylpyrrolidone, 30% ethylene glycol). One every two slides of each animal was stained with cresyl violet. Motoneurons were identified by their localization in the ventral horn and counted following strict size and morphological criteria: only neurons with diameter larger than 20 μm , polygonal shape and prominent nucleoli were counted. For each slide, the number of motoneurons present in both ventral horns was counted in four serial sections per slide of each L4 and L5 segments determined according to anatomical landmarks (Mancuso et al., 2011b). We calculated the total number of L4-L5 motoneurons by applying Abercrombie's correction (Abercrombie, 1946).

For morphological evaluation of axons, the tibial nerve was harvested and post-fixed in glutaraldehyde/paraformaldehyde (3%/3%) overnight at 4°C, post-fixed in 2% osmium tetroxide, dehydrated, and embedded in epon resin (Electron Microscopy Sciences, Hatfield, PA, USA). Transverse semithin sections (0.5 μm thick) were cut with an ultramicrotome (Leica), stained with toluidine blue, and examined by light microscopy.

For muscle immunohistochemistry, the gastrocnemius muscles were cryopreserved in 30% sucrose in PBS and 60 μm longitudinal sections were serially cut with a cryotome and collected in sequential series of 10 in Olmos solution. Sections were blocked with PBS-0.3% Triton-5% fetal bovine serum and incubated 48h at 4°C with primary antibodies anti-synaptophysin (1:500, AB130436, Abcam), anti-neurofilament 200 (NF200, 1:1000, AB5539, Millipore), anti-S100 β (1:1, 22520, Immunostar), anti-phospho-ErbB4 (1:100, sc-283, Santa Cruz Biotechnology), anti-phospho-Akt (1:50, Cell Signaling Technologies) and anti phospho-ERK1/2 (1:50, Cell Signaling Technologies). After washes, sections were incubated overnight with Alexa 594-conjugated secondary antibody (1:200; Life Science), Alexa 594-conjugated streptavidin (1:500, Life Science) and Alexa 488 conjugated α -bungarotoxin (1:200, B-13422, Life Technologies). To further amplify p-ErbB4 labeling, tyramide signal amplification (TSA) was applied (1:50, 5 minutes, NEL700001KT, Perking Elmer). All confocal images were captured with a scanning confocal microscope (LSM 700 Axio Observer, Carl Zeiss 40x/1.3 and 60x/1.4 Oil DIC M27). Maximum projections images shown in this study were generated from 0.5-2 μm z projections. For NMJ analysis, the proportion of fully occupied endplates was determined by classifying each endplate as

either fully occupied (when presynaptic terminals overly the endplate) or vacant (no presynaptic label in contact with the endplate). At least 4 fields totaling >100 endplates were analyzed per muscle. For collateral sprouting quantification, the number of sprouts per endplate was quantified by counting the neurofilament-positive projections from the pre-synaptic terminal or pre-terminal nodes on confocal z projections. For statistical analysis, we considered both the total number of sprouts and the proportion of occupied end plates that were originated from a collateral sprout (% of sprouts vs. occupied end plates). 3-D reconstructions were performed with Imaris software v. 8.2.0 (Bitplane AG) from z-stacks obtained from confocal microscopy.

RNA extraction and real time PCR

The gastrocnemius muscle was dissected, removed and divided in two parts. For RNA extraction 1000 μ l of Qiazol (Qiagen) were added, and tissue homogenized for 6 minutes with Tissue Lyser LT (Qiagen) at 50 Hz twice. Then, samples were purified with chloroform (Panreac), precipitated with isopropanol (Panreac), washed with 70% ethanol and resuspended in 20 μ l of RNase free water. The RNA concentration was measured using a NanoDrop ND-1000 (Thermo Scientific).

One μ g of RNA was reverse-transcribed using 10 μ mol/l DTT, 200 U M-MuLV reverse transcriptase (New England BioLabs, Barcelona, Spain), 10 U RNase Out Ribonuclease Inhibitor (Invitrogen), 1 μ mol/l oligo(dT), and 1 μ mol/l of random hexamers (BioLabs, Beverly, MA, USA). The reverse transcription cycle conditions were 25°C for 10 min, 42°C for 1 h and 72°C for 10 min. We analyzed the mRNA expression of murine ErbB4 by means of specific primer sets (forward: AGATCACCAGCATCGAGCAC, reverse: TGGTCTACATAGACTCCACC). m36B4 expression was used to normalize the expression levels of the different genes of interest for mouse samples (m36B4 forward: ATGGGTACAAGCGCGTCCTG, reverse: AGCCGCAAATGCAGATGGAT)

Gene-specific mRNA analysis was performed by SYBR-green real-time PCR using the MyiQ5 real-time PCR detection system (Bio-Rad Laboratories, Barcelona, Spain). The thermal cycling conditions comprised 5min polymerase activation at 95°C, 45 cycles of 15s at 95°C, 30s at 60°C, 30s at 72°C and 5s at 65°C to 95°C (increasing 0.5°C every 5s). Fluorescence detection was performed at the end of the PCR extension, and melting curves were analyzed by monitoring the continuous decrease in fluorescence of the SYBR Green signal. Quantification relative to 36B4 controls was calculated using the Pfaffl method (Pfaffl, 2001).

Protein extraction and western blot

The other part of the gastrocnemius muscle was prepared for protein extraction and homogenized in modified RIPA buffer (50 mM Tris–HCl pH 7.5, 1% Triton X-100, 0.5% sodium deoxycholate, 0.2% SDS, 100 mM NaCl, 1 mM EDTA) adding 10 μ l/ml of Protease Inhibitor cocktail (Sigma) and PhosphoSTOP phosphatase inhibitor cocktail (Roche). After clearance, protein concentration was measured by Lowry assay (Bio-Rad Dc protein assay).

For Western blots, 20–60 μ g of protein of each sample were loaded in SDS–polyacrylamide gels. The transfer buffer was 25 mM Trizma-base, 192 mM glycine, 20% (v/v) methanol, pH 8.4. The membranes were blocked with 5% BSA in PBS plus 0.1% Tween-20 for 1 hour, and then incubated with primary antibodies at 4°C overnight. The primary antibodies used were: anti-Neuregulin 1 (1:200, sc-228916, Santa Cruz Biotechnology), anti-ErbB4 (1:200, sc-283, Santa Cruz Biotechnology), anti-Akt (1:200, sc-8312, Santa Cruz Biotechnology), and-pAkt (1:200, sc-7985-R, Santa Cruz Biotechnology), anti-ERK1/2 (1:500, 4348, Cell Signaling), anti-pERK1/2 (1:500, 9106, Cell Signaling), anti-GSK3 β (1:500, ab31366, Abcam), anti-pGSK3 β (S9) (1:500, ab75814, Abcam), anti-GAPDH (1:20000, MAB374, Millipore). Horseradish peroxidase–coupled secondary antibody (1:5000, Vector) incubation was performed for 60 min at room temperature. The membranes were visualized using enhanced chemiluminescence method and the images were collected and analyzed with Gene Genome apparatus and Gene Snap and Gene Tools software (Syngene, Cambridge, UK).

Kinase phosphorylation assay (ELISA)

The phosphorylation levels of Akt and ERK1/2 was determined by the Phosphotracer ELISA kit (ab185432, Abcam) in a semi-quantitative method. We used RIPA homogenized mouse muscle and the amount of phosphorylated protein was determined according to the manufacturer instructions.

Human samples processing

Muscle biopsies were obtained from muscles of ALS patients (supplementary table 1) using an open biopsy after subcutaneous anesthesia, and the samples were immediately frozen in liquid nitrogen. Written informed consent was obtained from all participants and the research ethics committee from the institution approved the study. The biopsy sample from each individual was used to obtain RNA and protein extracts.

The RNA extraction was carried out using TriReagent (Sigma-Aldrich Co). The quality of the extracted RNA was checked in the NanoDrop spectrophotometer and 28S as well as 18S rRNA

bands were visualized in an agarose gel. The cDNA was obtained from 1 µg of total extracted RNA (High Capacity cDNA RT kit; Applied Biosystems). For ErbB4 mRNA expression analysis we used specific set of primers for ErbB4 (forward: CTTTAATTACCGCAGCCGCC, reverse: AAAGAGGCGGTAGGTTTCCG) and h36B4 for normalization (forward: ATGCAGCAGATCCGCATGT; reverse: TTGCGCATCATGGTGTCTT).

For protein analysis, muscle biopsies were homogenized in modified RIPA buffer (50 mM Tris-HCl pH 7.5, 1% Triton X-100, 0.5% sodium deoxycholate, 0.2% SDS, 100 mM NaCl, 1 mM EDTA) adding 10 µl/ml of Protease Inhibitor cocktail (Sigma) and PhosphoSTOP phosphatase inhibitor cocktail (Roche). After clearance, protein concentration was measured by BCA assay (Pierce). For Western blot, the experimental conditions were the same than those used for the analysis of murine samples. The antibody used was anti-ErbB4 (1:200, sc-283, Santa Cruz Biotechnology).

Statistics

All experiments were performed by blinded researchers using randomized animal groups. Data are expressed as mean ± SEM. Kolmogorov-Smirnov and Fisher tests were applied in order to determine the normality and the homogeneity of variances of data sets, respectively. Electrophysiological test results were statistically analyzed using one-way or repeated measurements ANOVA, applying Tukey post-hoc test when necessary. Histological and molecular biology data were analyzed using ANOVA and Tukey post-hoc, t-Student, or Kruskal-Wallis and Mann-Whitney tests.

Results

ErbB4 receptor is localized at the neuromuscular junction and down regulated in SOD1^{G93A} mice and ALS patients skeletal muscles

We first evaluated ErbB4 and ErbB2 expression along disease progression in SOD1^{G93A} muscles by real time PCR. We found a significant reduction of ErbB4 mRNA levels that correlates with the pattern of muscle denervation (Hegedus et al., 2007). ErbB4 mRNA was decreased from 8 weeks of age in gastrocnemius muscle and later, from 12 weeks, in soleus muscle, which is more resistant to the disease with delayed onset of denervation (**Fig. 1a**). Further immunohistochemical evaluation of mouse muscles showed that ErbB4 receptors were localized at the neuromuscular junction, being likely expressed in the terminal Schwann cells (**Fig. 1b**, note the co-labeling between ErbB4 and DAPI staining). On the contrary, the analysis of ErbB2 receptor in the gastrocnemius muscle revealed no changes along disease progression (**Fig. 1c**). We then analyzed human samples from sporadic and familial ALS patients (**supplementary table 1**) and found significantly decreased ErbB4 mRNA and protein levels compared to control values (**Fig. 1d**). Remarkably, ErbB4 protein levels were below 50% of normal expression in muscles of all ALS patients (**Fig. 1d, right panel**). This finding is in agreement with previous reports of loss-of-function ErbB4 mutations as causative of late-onset ALS (Takahashi et al., 2013).

AAV-Nrg1-I intramuscular injection promotes functional compensation by enhancing collateral sprouting in SOD1^{G93A} muscle.

In order to assess the role of Nrg1/ErbB pathway, we used a gene therapy strategy based on the bilateral intramuscular injection of 1×10^{11} viral genomes of an adeno-associated viral vector (AAV) encoding for soluble Nrg1-I (or GFP as a control) into SOD1^{G93A} gastrocnemius muscles previous to the clinical disease onset (at 8 weeks of age) (**Fig. 2a and b**). We first evaluated the GFP expression pattern in the muscles to determine which structures were transfected with the AAV and thereby expressed the transgene. We found that a high proportion of muscle fibers, but not axons or Schwann cells, were positive for GFP staining. In addition, we controlled the potential detrimental effect of the AAV-injection *per se* by functionally evaluating the effect of AAV-GFP intramuscular injection in SOD1^{G93A} mice, and found no alterations derived by the virus injection in the outcome of the animals (**Supplementary fig. 1**).

Induced Nrg1-I expression was confirmed in the animals at the time of sacrifice (16 weeks), showing significantly higher levels of Nrg1-I in the gastrocnemius muscles injected compared to untreated wild type and SOD1^{G93A} mice (**Fig. 2c**). The functional effect of AAV-Nrg1-I injection

was evaluated in the hindlimb muscles of SOD1^{G93A} mice by means of electrophysiological tests, which have been demonstrated to reliably monitor disease progression in ALS patients and animal models (Azzouz et al., 1997; Shefner et al., 2006; Mancuso et al., 2011b). Results revealed a selective preservation of the gastrocnemius compound muscle action potential (CMAP) from 10 weeks of age, without affecting adjacent non-injected muscles, such as the tibialis anterior muscle (**Fig. 2d**). The preserved CMAP amplitude might result from increasing either the number or the size of motor units by collateral sprouting, a compensatory mechanism by which intact motoneurons expand to reinnervate denervated endplates on muscle fibers (Tam and Gordon, 2003b). We estimated the size and number of motor units by the incremental technique and found that Nrg1-I overexpression had no effect regarding the number of motor units, but significantly increased motor unit mean amplitude. The frequency distribution of motor units grouped by amplitude of the action potential revealed a clear shift to the right in the Nrg1-I treated animals, corroborating the increased size of motor units (**Fig. 2e**). Further histological analysis confirmed these findings since the treatment had effect neither on total motoneuron preservation at L4-L5 spinal segments nor on myelinated axons at the tibial nerve (**Fig. 2f**, top and middle panels), but higher number of occupied motor endplates were observed in the gastrocnemius muscle after AAV-Nrg1-I injection compared to untreated SOD1^{G93A} mice (**Fig. 2f**, bottom panel). We also observed an increased proportion of occupied endplates by terminal and nodal collateral sprouts and a higher number of sprouting profiles in treated muscles (**Fig. 2g**). The enhanced collateral sprouting in Nrg1-I treated muscles was confirmed by the presence of terminal Schwann cells extending processes to neighbor end plates (**Fig. 2h**), which have been shown to be essential for the guidance of new axonal sprouts (Kang et al., 2014).

These findings confirm the hypothesis of Nrg1-I increasing the number of neuromuscular connections by promoting collateral sprouting and reinnervation. Nevertheless, the increased functionality of just the gastrocnemius muscles was not enough for improving the global disease outcome of the animals, evidenced by the lack of differences in the rotarod performance or the clinical disease onset (**Fig. 3**).

To better mimic a clinical situation, we studied another group of SOD1^{G93A} mice injected with AAV-Nrg1-I at 12 weeks of age, the usual time of clinical onset of the disease in this model (Ripps et al., 1995; Mancuso et al., 2011a; 2011b). Results revealed also significant preservation of gastrocnemius CMAP amplitude, accompanied by increased size of motor units potential amplitude and a higher percentage of occupied endplates (**Fig. 4**), thereby confirming the beneficial effect of Nrg1-I overexpression even when applied at a stage of higher degree of muscle denervation.

AAV-Nrg1-I effect is mediated by the activation of Akt and ERK1/2 dependent pathways

We next analyzed the signaling pathways underlying the effect observed upon Nrg1-I overexpression in SOD1^{G93A} mice muscles. We found increased ErbB4 protein levels in AAV-Nrg1-I injected mice at 16 weeks, together with an increased phosphorylation of the receptor in terminal Schwann cells at the neuromuscular junction (**Fig. 5a and b**). We performed orthogonal views from confocal microscopy z-stacks and 3D reconstructions in order to confirm ErbB4 localization, and found that it is present in the surface of terminal Schwann cells, indicating that these cells are the main target of the enforced Nrg1-1 expression (**Fig. 5c and d**). To corroborate the functional activation of ErbB receptors through Nrg1 signaling we analyzed changes in the phosphorylation levels of Akt, ERK1/2, and GSK3 β , members of the MAPK family known to be downstream of ErbB (Mei and Xiong, 2008; Fledrich et al., 2014). We found activation of both Akt and ERK1/2, evidenced by the relative higher phosphorylated form compared to total protein in AAV-Nrg1-I injected muscles (**Fig. 5e, g and i**). Interestingly, further immunohistochemical analysis revealed a restricted activation of ERK1/2 co-localizing with the motor endplate, and Akt in skeletal muscle fibers (**Fig. 5f and h**). In addition, the enhanced Akt activation was confirmed by the inhibition of GSK3 β , as indicated by the increased inhibitory S9 specific phosphorylation (**Fig. 5i**). Such Akt-dependent beneficial effect was recently reported for soluble Nrg1-I on Schwann cells in a Charcot-Marie-Tooth 1A rat model (Fledrich et al., 2014).

Nrg1/ErbB signaling pathway plays a crucial role in motor collateral sprouting

To further understand the role of Nrg1 on axonal collateral sprouting, we used a model of hindlimb muscle partial denervation, consisting in postganglionic axotomy of the L4 spinal nerve (rhizotomy) in wild type mice (Gordon et al., 2010) (**Fig. 6a**). ErbB4 receptor mRNA levels in partially and completely denervated muscles were significantly reduced after 3 days compared to naive animals (**Fig. 6b**). We histologically and functionally characterized the effect of the L4 rhizotomy. Tibial nerve histology at 15 days revealed a significant decrease of approximately 30% of myelinated axons (**Fig. 6c**). Electrophysiological tests showed that tibialis anterior and gastrocnemius CMAPs dropped to 65 and 55% and progressively recovered to 90 and 95% of naive values, respectively (**Fig. 6d**), although there were no clear functional alterations in behavior (data not shown). These data correlates with previous studies showing similar percentages of muscle innervation after selective L4/L5 avulsion in male mice (Gordon et al., 2012). Therefore, this model allows consistent partial denervation of selected muscles and fast recovery of neuromuscular

function due to collateral reinnervation. Next, we studied three rhyzotomy experimental groups intramuscularly injected with 1×10^{11} vg of AAV1-Nrg1-I (14 days prior to injury), with lapatinib (an ErbB receptor tyrosine kinase activity inhibitor) or with vehicle (**Fig. 7a**). Results revealed that Nrg1-I overexpression enhanced the recovery of gastrocnemius CMAP by accelerating collateral reinnervation, but without altering the maximum compensatory enlargement of each motor unit, evidenced by the lack of differences in the mean motor unit potential amplitude at late time points. On the contrary, ErbB inhibition by lapatinib completely blocked functional recovery of gastrocnemius muscle CMAP by inhibiting collateral sprouting and the increase of motor units size (**Fig. 7a and b**). Histological analysis at 15 days after rhyzotomy confirmed these results since lapatinib-treated animals showed reduced percentage of occupied muscle endplates and few collateral sprouts. In addition, the lack of histological differences between Nrg1-I and vehicle groups confirms that Nrg1-I accelerates collateral sprouting rather than increases the maximum motor unit compensatory capacity (**Fig. 7c and d**). Although Nrg-1-I has been already related to peripheral nerve regeneration mainly by its actions on Schwann cells (Stassart et al., 2012), this is the first report demonstrating an important role of Nrg1-I in the collateral sprouting process. A note of caution might be taken for lapatinib treatment, since this drug is not specific for ErbB4 receptors and the observed effect may be explained in part by blocking of other ErbB receptor subtypes.

Nrg1 effect on collateral sprouting is also dependent on the activation of Akt and ERK1/2.

We further analyzed Nrg1-I and ErbB4 expression levels and activation of MAPK signaling pathways in the rhyzotomy model. As expected, Nrg1-I levels increased in the muscles injected with AAV-Nrg1-I. Surprisingly, we also found slight increase of endogenous Nrg1-I after rhyzotomy in vehicle-injected muscles that was reduced by lapatinib. We did not find differences in ErbB4 expression after AAV-Nrg1-I administration, but ErbB4 levels were markedly reduced by lapatinib treatment, probably due to the lower levels of muscle innervation in this case. MAPK analyses revealed no significant effect of Nrg1-I overexpression in terms of Akt and ERK1/2 phosphorylation after rhyzotomy. In contrast, lapatinib administration led to a dramatic decrease of both Akt and ERK1/2 activity (**Fig. 7e**).

Discussion

It was recently reported that loss-of-function mutations on the Nrg1 receptor ErbB4 produce a form of late-onset, autosomal-dominant ALS in humans (Takahashi et al., 2013), opening a new field for searching novel therapeutic approaches. Thereby, the main goal of the present work was to determine the role of soluble Nrg1-I in ALS by assessing the effect of its overexpression at the NMJs in SOD1^{G93A} mice. Our novel results show that Nrg1-I plays an important role for collateral sprouting of motor axons and reinnervation of partially denervated muscles, and that overexpression of Nrg1-I by an AAV vector promotes functional compensation in SOD1^{G93A} mouse muscles by enhancing collateral reinnervation.

ALS is a multifactorial disease in which a complex network of pathophysiological processes results in the progressive degeneration of motoneurons (Mancuso and Navarro, 2015). Many efforts are directed to therapeutically target one or more of these pathophysiological events in order slow-down ALS disease progression (Mancuso and Navarro, 2015). Motoneuron death is preceded by failure of NMJs and axonal retraction (Fischer et al., 2004; Mancuso et al., 2011b), which seem dependent upon alterations in the interaction of motor axons with accompanying terminal Schwann cells and skeletal muscle fibers. Importantly, we show for the first time that Nrg1-I overexpression in SOD1^{G93A} mice produced significant functional compensation by enhancing collateral sprouting by acting on terminal Schwann cells, thus inducing active functional recovery rather than preservation of motoneurons.

Many efforts have been conducted to elucidate the role of Nrg1 in the peripheral nervous system. However, most of them were mainly focused on the Nrg1 type III (Nrg1-III) (Esper et al., 2006; Nave and Salzer, 2006; Mei and Xiong, 2008). It has been shown that Nrg1-III enhances remyelination and regeneration by stimulating Schwann cells migration after nerve injury in the adulthood (Fricker et al., 2011; Wakatsuki et al., 2013). Moreover, it has been suggested that this effect was dependent upon endogenous BDNF signaling through axonal trkB receptors, which promote a stage-dependent release of Nrg1-III from axons to Schwann cells (Ma et al., 2011). Nrg1-III has been also reported to have an important effect on central nervous system myelination by inducing the proliferation of oligodendrocyte precursors (Ortega et al., 2012) and even oligodendrocyte replacement and maintenance after spinal cord injury, leading to improved functional outcome (Gauthier et al., 2013).

Despite the important role of Nrg1-III on peripheral nervous system development and regeneration after traumatic injuries, the exact role of Nrg1-I on the peripheral nervous system is not fully known. Recent findings suggest that it also contributes to axonal maintenance and

regeneration. Cheret et al. (Cheret et al., 2013) recently showed that Nrg1 alterations produce severe deficits in the formation and maturation of muscle spindles, thereby compromising the proprioceptive sensory system. After nerve injury, Schwann cell detachment from axons triggers Nrg1-I expression that is essential for promoting axonal regeneration and remyelination (Stassart et al., 2012). Interestingly, Nrg1-I induces Schwann cells proliferation after peripheral nerve injury through ERK activation (Lee et al., 2014). Most importantly, beneficial effects of Nrg1-I administration have been recently observed in a rodent model of Charcot-Marie-Tooth disease, in which axonal Nrg1-I overexpression drives Schwann cells towards differentiation and preserves peripheral axons through PI3K-Akt signaling (Fledrich et al., 2014). We provide the first evidence of the role of Nrg1-I in collateral sprouting on partially denervated muscles. We showed how Nrg1-I is able to activate ErbB4 receptors present in terminal Schwann cells at the neuromuscular junction, and induce active collateral reinnervation. Chronic blockade of ErbB receptors abolishes this process. Our present results on the critical role of Nrg1-I in the process of motor axon collateral sprouting and reinnervation of vacant NMJ are in agreement with previous findings reporting Nrg1-I effect on Schwann cells through the activation of MAPK pathways (Fledrich et al., 2014). In this sense, Nrg1-I has been shown to be also critical for the stability of AChRs at the NMJ and the structural integrity of the postsynaptic apparatus (Schmidt et al., 2011). Interestingly, knockdown of axonally-derived Nrg1-III produced severe impairment of remyelination after sciatic nerve crush, together with excessive terminal sprouting observed at the NMJ level (Wolpowitz et al., 2000). These findings might suggest an opposite action of Nrg1-I and Nrg1-III in terms of modulating motor axonal sprouting. However, the excess terminal sprouting after Nrg1-III silencing might be a compensatory reaction to the grossly impaired remyelination of the motor axons rather than a direct consequence of the absence of Nrg1-III at the NMJ. Indeed, increased NMJ terminal sprouting has been also described in a transgenic mouse model of demyelinating neuropathy as a consequence of demyelination and conduction block (Baloh et al., 2009).

Although the molecular mechanisms underlying collateral sprouting are still unknown, the cellular events taking place in the process have been well studied. Terminal Schwann cells in denervated NMJ are able to extend processes and migrate towards neighbor occupied end plates. Then, growing collateral and terminal sprouts from preserved motor axons follow these Schwann cell processes to reinnervate the vacant end plates (Tam and Gordon, 2003b; Harrisinigh et al., 2004; Kang and Thompson, 2003; Kang et al., 2014). Remarkably, we observed that phospho-ErbB4 expression is located at the surface of terminal Schwann cells upon Nrg1-I enforced expression in the muscles (see figure 5b). Our results demonstrate that Nrg1-I acts on terminal Schwann cells,

likely enhancing its role as bridges for the collateral reinnervation of muscle fibers. The induction of a constitutively active receptor ErbB2 in Schwann cells, simulating continuous neuregulin signaling to these cells, was reported to lead to changes in terminal Schwann cells that mimicked the response to muscle denervation/reinnervation (Hayworth et al., 2006). This activation of Schwann cells resulted in the sprouting of nerve terminals following the extensions of the terminal Schwann cells.

Our results also reveal an activation of ERK1/2 in motor endplates of Nrg1-I treated muscles. In this sense, it has been shown that ERK is crucial for the events occurring in Schwann cells after peripheral nerve injury, including proliferation, migration and remyelination. Following nerve injury, Schwann cells respond to axonal damage with a strong, sustained activation of the ERK signaling pathway (Harrisingh et al., 2004). In addition, sustained Raf/MEK/ERK signaling triggered in Schwann cells is able to switch their condition into a proliferative, remyelinating state even when interacting with intact axons (Napoli et al., 2012). Overall, our findings suggest that Nrg1-I overexpression is able to enhance collateral reinnervation of empty motor endplates by acting on terminal Schwann cells in an ERK1/2 dependent manner.

A note of caution might be taken regarding the lack of global effects observed in the functional outcome of Nrg1-I treated ALS mice. It is unlikely that Nrg1-I enforcement in single muscles would globally affect ALS disease progression, but we believe that our findings of increased collateral reinnervation in SOD1^{G93A} mice with enhanced Nrg1-I expression represents a crucial step forward the development of new therapies for motoneuron disease. In this sense, our work constitutes a convincing proof of concept that establishes the basis for investigating the therapeutic impact of Nrg1-I widespread expression in ALS models.

In conclusion, the present results demonstrate an important role of Nrg1-I on axonal sprouting and muscle collateral reinnervation. Nrg1-I overexpression in SOD1^{G93A} mice produced significant functional compensation by promoting collateral reinnervation, thereby opening a new window for developing new therapies focusing on functional recovery rather than preservation for motoneuron diseases.

Acknowledgments

This work was supported by grant TV3201428-10 of Fundació La Marato-TV3, grants PI14/00947, PI10/00092, PI14/00088, PI111532, PS09720 and PS09730, TERCEL and CIBERNED funds from the Fondo de Investigación Sanitaria of Spain, Instituto de Salud Carlos III, grant SAF2009-12495 from the Ministerio de Ciencia e Innovación of Spain, grants 2014SGR-1354 and 2014SGR-201 from the Generalitat de Catalunya, grant Nrg14ALS of AFM-Telethon, FEDER funds, and Gobierno de Aragón. RM is recipient of a predoctoral fellowship from the Ministerio de Educación of Spain. We appreciate the technical help of Jessica Jaramillo in the histological studies. We thank the Vector Production Unit at CBATEG (Universitat Autònoma de Barcelona) for producing AAV vectors, the LLEB (UAB) for the luminescence measurements, and Dr. James M. Wilson (University of Pennsylvania) for providing AAV1 RepCap plasmids.

Declaration of interest

The authors report no conflicts of interest. The authors alone are responsible for the content and writing of the paper.

References

- Abercrombie M (1946) Estimation of nuclear population from microtome sections. *Anat Rec* 94:239–247.
- Andersen PM, Al-Chalabi A (2011) Clinical genetics of amyotrophic lateral sclerosis: what do we really know? *Nat Rev Neurol* 7:603–615.
- Azzouz M, Leclerc N, Gurney M, Warter JM, Poindron P, Borg J (1997) Progressive motor neuron impairment in an animal model of familial amyotrophic lateral sclerosis. *Muscle Nerve* 20:45–51.
- Baloh RH, Strickland A, Ryu E, Le N, Fahrner T, Yang M, Nagarajan R, Milbrandt J (2009) Congenital hypomyelinating neuropathy with lethal conduction failure in mice carrying the *Egr2* I268N mutation. *J Neurosci* 29:2312–2321.
- Bosco DA, Morfini G, Karabacak NM, Song Y, Gros-Louis F, Pasinelli P, Goolsby H, Fontaine BA, Lemay N, McKenna-Yasek D, Frosch MP, Agar JN, Julien JP, Brady ST, Brown RH (2010) Wild-type and mutant SOD1 share an aberrant conformation and a common pathogenic pathway in ALS. *Nat Neurosci* 13:1396–1403.
- Cheret C, Willem M, Fricker FR, Wende H, Wulf-Goldenberg A, Tahirovic S, Nave K-A, Saftig P, Haass C, Garratt AN, Bennett DL, Birchmeier C (2013) *Bace1* and *Neuregulin-1* cooperate to control formation and maintenance of muscle spindles. *EMBO J* 32:2015–2028.
- DeJesus-Hernandez M et al. (2011) Expanded GGGGCC hexanucleotide repeat in noncoding region of *C9ORF72* causes chromosome 9p-linked FTD and ALS. *Neuron* 72:245–256.
- Esper RM, Pankonin MS, Loeb JA (2006) *Neuregulins*: Versatile growth and differentiation factors in nervous system development and human disease. *Brain Res Rev* 51:161–175.
- Fischer LR, Culver DG, Tennant P, Davis AA, Wang M, Castellano-Sanchez A, Khan J, Polak MA, Glass JD (2004) Amyotrophic lateral sclerosis is a distal axonopathy: evidence in mice and man. *Exp Neurol* 185:232–240.
- Fischer LR, Li Y, Asress SA, Jones DP, Glass JD (2012) Absence of SOD1 leads to oxidative stress in peripheral nerve and causes a progressive distal motor axonopathy. *Exp Neurol* 233:163–171.
- Fledrich R, Stassart RM, Klink A, Rasch LM, Prukop T, Haag L, Czesnik D, Kungl T, Abdelaal TAM, Keric N, Stadelmann C, Brück W, Nave K-A, Sereda MW (2014) Soluble *neuregulin-1* modulates disease pathogenesis in rodent models of Charcot-Marie-Tooth disease 1A. *Nat Med* 20:1055–1061.
- Frey D, Schneider C, Xu L, Borg J, Spooren W, Caroni P (2000) Early and selective loss of neuromuscular synapse subtypes with low sprouting competence in motoneuron diseases. *J Neurosci* 20:2534–2542.
- Fricker FR, Lago N, Balarajah S, Tsantoulas C, Tanna S, Zhu N, Fageiry SK, Jenkins M, Garratt AN, Birchmeier C, Bennett DLH (2011) Axonally derived *neuregulin-1* is required for remyelination and regeneration after nerve injury in adulthood. *J Neurosci* 31:3225–3233.

- Gauthier M-K, Kosciuczyk K, Tapley L, Karimi-Abdolrezaee S (2013) Dysregulation of the neuregulin-1-ErbB network modulates endogenous oligodendrocyte differentiation and preservation after spinal cord injury. *Eur J Neurosci* 38:2693–2715.
- Gordon T, Tyreman N, Li S, Putman CT, Hegedus J (2010) Functional over-load saves motor units in the SOD1-G93A transgenic mouse model of amyotrophic lateral sclerosis. *Neurobiol Dis* 37:412–422.
- Graffmo KS, Forsberg K, Bergh J, Birve A, Zetterström P, Andersen PM, Marklund SL, Brännström T (2013) Expression of wild-type human superoxide dismutase-1 in mice causes amyotrophic lateral sclerosis. *Hum Mol Genet* 22:51–60.
- Gurney ME, Pu H, Chiu AY, Dal Canto MC, Polchow CY, Alexander DD, Caliando J, Hentati A, Kwon YW, Deng HX (1994) Motor neuron degeneration in mice that express a human Cu,Zn superoxide dismutase mutation. *Science* 264:1772–1775.
- Harrisingh MC, Perez-Nadales E, Parkinson DB, Malcolm DS, Mudge AW, Lloyd AC (2004) The Ras/Raf/ERK signalling pathway drives Schwann cell dedifferentiation. *EMBO J* 23:3061–3071.
- Hayworth CR, Moody SE, Chodosh LA, Krieg P, Rimer M, Thompson WJ (2006) Induction of neuregulin signaling in mouse Schwann cells in vivo mimics responses to denervation. *J Neurosci* 26:6873–6884.
- Hegedus J, Putman CT, Gordon T (2007) Time course of preferential motor unit loss in the SOD1 G93A mouse model of amyotrophic lateral sclerosis. *Neurobiol Dis* 28:154–164.
- Kang H, Thompson WJ (2003) Terminal Schwann cells guide the reinnervation of muscle after nerve injury. *J Neurocytol* 32:975–985.
- Kang H, Tian L, Mikesch M, Lichtman JW, Thompson WJ (2014) Terminal Schwann cells participate in neuromuscular synapse remodeling during reinnervation following nerve injury. *J Neurosci* 34:6323–6333.
- Kiernan MC, Vucic S, Cheah BC, Turner MR, Eisen A, Hardiman O, Burrell JR, Zoing MC (2011) Amyotrophic lateral sclerosis. *The Lancet* 377:942–955.
- Lago N, Rodríguez FJ, Guzmán MS, Jaramillo J, Navarro X (2007) Effects of motor and sensory nerve transplants on amount and specificity of sciatic nerve regeneration. *J Neurosci Res* 85:2800–2812.
- Lee HJ, Shin YK, Park HT (2014) Mitogen activated protein kinase family proteins and c-jun signaling in injury-induced Schwann cell plasticity. *Exp Neurol* 23:130.
- Ma Z, Wang J, Song F, Loeb JA (2011) Critical period of axoglial signaling between neuregulin-1 and brain-derived neurotrophic factor required for early Schwann cell survival and differentiation. *J Neurosci* 31:9630–9640.
- Mancuso R, Navarro X (2015) Amyotrophic lateral sclerosis: Current perspectives from basic research to the clinic. *Prog Neurobiol* 133:1–25
- Mancuso R, Oliván S, Osta R, Navarro X (2011a) Evolution of gait abnormalities in SOD1(G93A)

transgenic mice. *Brain Res* 1406:65–73.

Mancuso R, Santos-Nogueira E, Osta R, Navarro X (2011b) Electrophysiological analysis of a murine model of motoneuron disease. *Clin Neurophysiol* 122:1660–1670.

Mei L, Xiong W-C (2008) Neuregulin 1 in neural development, synaptic plasticity and schizophrenia. *Nat Rev Neurosci* 9:437–452.

Napoli I, Noon LA, Ribeiro S, Kerai AP, Parrinello S, Rosenberg LH, Collins MJ, Harrisingh MC, White IJ, Woodhoo A, Lloyd AC (2012) A central role for the ERK-signaling pathway in controlling Schwann cell plasticity and peripheral nerve regeneration in vivo. *Neuron* 73:729–742.

Navarro X, Udina E (2009) Methods and protocols in peripheral nerve regeneration experimental research. Part III – Electrophysiological evaluation. *Int Rev Neurobiol* 87:105–126.

Nave K-A, Salzer JL (2006) Axonal regulation of myelination by neuregulin 1. *Current Opinion Neurobiol* 16:492–500.

Ngo ST, Cole RN, Sunn N, Phillips WD, Noakes PG (2012) Neuregulin-1 potentiates agrin-induced acetylcholine receptor clustering through muscle-specific kinase phosphorylation. *J Cell Sci* 125:1531–1543.

Ortega MC, Bribián A, Peregrín S, Gil MT, Marín O, de Castro F (2012) Neuregulin-1/ErbB4 signaling controls the migration of oligodendrocyte precursor cells during development. *Exp Neurol* 235:610–620.

Pfaffl MW (2001) A new mathematical model for relative quantification in real-time RT-PCR. *Nucleic Acids Res* 29:45e–45.

Renton AE et al. (2011) A Hexanucleotide Repeat expansion in C9ORF72 is the cause of chromosome 9p21-linked ALS-FTD. *Neuron* 72:257–268.

Ripps ME, Huntley GW, Hof PR, Morrison JH, Gordon JW (1995) Transgenic mice expressing an altered murine superoxide dismutase gene provide an animal model of amyotrophic lateral sclerosis. *Proc Natl Acad Sci USA* 92:689–693.

Schmidt N, Akaaboune M, Gajendran N, Martinez-Pena y Valenzuela I, Wakefield S, Thurnheer R, Brenner HR (2011) Neuregulin/ErbB regulate neuromuscular junction development by phosphorylation of α -dystrobrevin. *J Cell Biol* 195:1171–1184.

Shefner JM, Cudkovicz M, Brown RH (2006) Motor unit number estimation predicts disease onset and survival in a transgenic mouse model of amyotrophic lateral sclerosis. *Muscle Nerve* 34:603–607.

Song F, Chiang P, Wang J, Ravits J, Loeb JA (2012) Aberrant neuregulin 1 signaling in amyotrophic lateral sclerosis. *J Neuropathol Exp Neurol* 71:104.

Stassart RM, Fledrich R, Velanac V, Brinkmann BG, Schwab MH, Meijer D, Sereda MW, Nave K-A (2012) A role for Schwann cell-derived neuregulin-1 in remyelination. *Nat Neurosci* 16:48–54.

Takahashi Y et al. (2013) ERBB4 Mutations that disrupt the neuregulin-ErbB4 pathway cause amyotrophic lateral sclerosis Type 19. *Am J Hum Genet* 93:900–905.

Tam SL, Gordon T (2003a) Neuromuscular activity impairs axonal sprouting in partially denervated muscles by inhibiting bridge formation of perisynaptic Schwann cells. *J Neurobiol* 57:221–234.

Tam SL, Gordon T (2003b) Mechanisms controlling axonal sprouting at the neuromuscular junction. *J Neurocytol* 32:961–974.

Trachtenberg JT, Thompson WJ (1996) Schwann cell apoptosis at developing neuromuscular junctions is regulated by glial growth factor. *Nature* 379:174–177.

Trojan DA, Gendron D, Cashman NR (1991) Electrophysiology and electrodiagnosis of the post-polio motor unit. *Orthopedics* 14:1353–1361.

Turner MR, Hardiman O, Benatar M, Brooks BR, Chio A, de Carvalho M, Ince PG, Lin C, Miller RG, Mitsumoto H (2013) Controversies and priorities in amyotrophic lateral sclerosis. *Lancet Neurol* 12:310–322.

Wakatsuki S, Araki T, Sehara-Fujisawa A (2013) Neuregulin-1/glial growth factor stimulates Schwann cell migration by inducing $\alpha 5 \beta 1$ integrin-ErbB2-focal adhesion kinase complex formation. *Genes Cells* 19:66–77.

Wolpowitz D, Mason T, Dietrich P, Mendelsohn M, Talmage DA, Role LW (2000) Cysteine-rich domain isoforms of the neuregulin-1 gene are required for maintenance of peripheral synapses. *Neuron* 25:79–91.

Figure legends

Figure 1. ErbB4 expression in muscles from SOD1^{G93A} mice and ALS patients. (a) Real time PCR analysis of ErbB4 mRNA in SOD1^{G93A} mice showed downregulation with a different pattern depending upon the analyzed muscle. The gastrocnemius muscle (GCm) showed marked ErbB4 mRNA reduction from 8 weeks of age, whereas the more ALS-resistant soleus muscle showed ErbB4 mRNA reduction from 12 weeks of age (n=3 animals per group and time point, ANOVA **p<0.01 vs. control). (b) Representative confocal images of ErbB4 expression at the neuromuscular junction in the mouse. The observed pattern of expression points to a terminal Schwann cell localization (scale bar = 10µm). (c) ErbB2 mRNA expression showing no differences along disease progression in gastrocnemius muscle of SOD1^{G93A} mice. (d) Real time PCR from samples of patients affected by sporadic or familial ALS showed reduced ErbB4 mRNA levels compared to control subjects, consistent with a severe reduction of ErbB4 protein levels (t-Student test, *p<0.05; ***p<0.001 vs. control). Numbers in parentheses indicate the number of tissue samples analyzed. Values are represented as mean±SEM. Individual levels of ErbB4 protein in each ALS patient are shown in the right panel. Additional information about patients features is provided in the supplementary table 1.

Figure 2. Effect of intramuscular AAV-Nrg1-I injection in SOD1^{G93A} mice. (a) Expression cassette and (b) representation of the administration procedure in the gastrocnemius muscle. (c) Nrg1-I protein levels were largely increased in the AAV-Nrg1-I injected muscles (n=10 animals per group with balanced sexes; one-way ANOVA, ***p<0.001 vs. wild type (wt) and SOD1^{G93A} untreated mice (SOD1c). (d) Electrophysiological tests revealed that AAV-Nrg1-I injection produced preservation of the amplitude of gastrocnemius CMAP in treated animals from 10 weeks of age (n= 20 animals per group, balanced sexes; repeated measurements ANOVA, **p<0.01; ***p<0.001 vs. SOD1 untreated mice). In contrast there were no differences between treated and control SOD1 mice in the amplitude of CMAP recorded in the tibialis anterior muscle (non-injected) along time. (e) Electrophysiological estimation of motor unit number (MUNE) and mean amplitude of single motor unit potential (SMUA) of the gastrocnemius muscle revealed that the increased CMAP amplitude was the result of increased size of motor units (t-Student test, ***p<0.001 vs. SOD1 untreated mice). This was confirmed by the shift to the left in the frequency distribution plot of motor unit potential amplitude in the animals treated with AAV-Nrg1-I (Chi-

square test, $p < 0.05$). (f) Histological analysis showed similar loss in the number of motoneurons in the ventral horn of the spinal cord (Nissl staining; top panels, scale bar = $250\mu\text{m}$), and in the number of myelinated fibers of the tibial nerve (semithin sections stained with toluidine blue; mid panels, scale bar = $10\mu\text{m}$) in treated and untreated $\text{SOD1}^{\text{G93A}}$ mice. Immunohistochemical labeling for axons (NF-200 and synaptophysin) and end plates (α -bungarotoxin) of the gastrocnemius muscle of 16 weeks-old $\text{SOD1}^{\text{G93A}}$ mice revealed a significantly increased number of occupied motor endplates after AAV-Nrg1-I injection ($n=10$ animals per group, balanced sexes; one-way ANOVA, $**p < 0.01$ vs. wild type; $##p < 0.01$ vs. untreated SOD1 mice; scale bar = $250\mu\text{m}$). (g) Representative images of nodal and terminal sprouts (pointed by arrowheads) from motor axons in the gastrocnemius muscle of $\text{SOD1}^{\text{G93A}}$ mice injected with AAV-Nrg1-I (scale bar = $15\mu\text{m}$). Higher numbers of terminal and nodal collateral sprouts were counted in $\text{SOD1}^{\text{G93A}}$ mice treated with AAV-Nrg1-I than in untreated $\text{SOD1}^{\text{G93A}}$ mice (t-Student test, $**p < 0.01$ vs. untreated SOD1 mice). (h) Representative confocal microphotographs of terminal Schwann cells (S100) extending processes to connect motor endplates in AAV-Nrg1-I injected muscles. Arrowheads point to terminal Schwann cell bodies (scale bar = $15\mu\text{m}$). For all graphs, values are $\text{mean} \pm \text{SEM}$.

Figure 3. Effect of Nrg1-I overexpression on functional outcome of $\text{SOD1}^{\text{G93A}}$ mice. Enhanced expression of Nrg1-I exclusively localized in the gastrocnemius muscle was not able to improve the global functional outcome of the animals neither in (a) the rotarod nor in (b) the clinical disease onset.

Figure 4. AAV-Nrg1-I injection in $\text{SOD1}^{\text{G93A}}$ gastrocnemius muscle at 12 weeks of age. (a) AAV-Nrg1-I injection at 12 weeks of age promotes slight but significant increase in the gastrocnemius muscle compound action potential (CMAP) ($n= 8$ treated vs. 20 untreated animals; repeated measures ANOVA, $*p < 0.05$ vs. SOD1 untreated mice), accompanied by an increase in the single motor unit potential amplitude (SMUA) (t-Student test). (b) Immunohistochemical labeling of axons and endplates of the gastrocnemius muscle showed increased proportion of occupied endplates after the Nrg1-I treatment ($n= 8$ treated vs. 10 untreated animals; t-Student test). Values are $\text{mean} \pm \text{SEM}$.

Figure 5. Nrg1-I enforced expression targets terminal Schwann cells in $\text{SOD1}^{\text{G93A}}$ mice gastrocnemius muscle. (a) Western blot analysis indicated partially recovered ErbB4 expression after Nrg1-I treatment ($n=10$ animals per group, balanced sexes). (b) Representative confocal

images showing pErbB4 expression in terminal Schwann cells of Nrg1-I treated animals. Scale bar = 10 μ m. (c) Orthogonal views confirmed the co-localization of pErbB4 in terminal Schwann cells, and (d) 3-D reconstructions from confocal z-stacks showed pErbB4 in the plasma membrane of these cells. Scale bar = 10 μ m. (e) Western blot of muscle samples revealed a significant activation of ERK1/2 after Nrg1-I overexpression, whereas (f) further IHC analysis revealed restricted ERK1/2 phosphorylation in the neuromuscular junction of treated animals, with a pattern of staining consistent with Schwann cells localization and morphology. (g) Western blot of muscle samples revealed a significant activation Akt after Nrg1-I overexpression, whereas (h) further IHC analysis revealed restricted Akt phosphorylation in skeletal muscle fibers. (i) Increased activation of ERK1/2 and Akt in Nrg1-I treated muscles was confirmed by ELISA, and by the phosphorylation of GSK3 β . Scale bars are 10 μ m. Values are mean \pm SEM. For all plots, one-way ANOVA test, # p<0.05 vs. untreated wild type; * p<0.05 vs. untreated SOD1^{G93A} mice.

Figure 6. L4 rhyzotomy model characterization. (a) Representation of the postganglionic L4 rhyzotomy. (b) ErbB4 mRNA levels were downregulated at 5 days post injury in gastrocnemius muscle after partial (L4 rhyzotomy) and total (sciatic nerve cut) denervation (n=4-5 animals per group, ANOVA, **p<0.05 vs. naive mice). (c) Tibial nerve histology revealed approximately 30% loss of myelinated axons (n=4-5 animals per group, t-Student test, *p<0.05 vs. naive mice, scale bar = 10 μ m). (d) Compound muscle action potential (CMAP) recordings showed no alteration of plantar muscles (innervated by L5-L6 ventral roots), but a marked drop to 65 and 55% of normal values for tibialis anterior and gastrocnemius muscles (innervated by L4-L5 ventral roots) that progressively recovered until reaching 90 and 95%, respectively (n=10).

Figure 7. Nrg1-I/ErbB signaling plays a role in collateral sprouting of motor axons. (a) The amplitude of the CMAP of the partially denervated gastrocnemius muscle recovered to normal values in AAV-Nrg1-I injected mice faster than in vehicle-injected mice, indicating acceleration of the collateral reinnervation. In contrast, lapatinib (ErbB inhibitor) injection completely prevented collateral reinnervation (n = 10 vehicle, 9 AAV-Nrg1-I and 8 lapatinib administered mice; One-way ANOVA, *p<0.05, ***p<0.001 AAV-Nrg1-I vs. vehicle treated animals; ###p<0.001 AAV-Nrg1-I vs. lapatinib treated animals; @@@p<0.001 lapatinib vs. vehicle treated animals). (b) The amplitude of single motor unit potentials (SMUA) of the gastrocnemius muscle was similarly increased in vehicle and AAV-Nrg1-I injected mice, but remained lower in lapatinib injected mice, indicating that ErbB blocking prevented collateral reinnervation (*p<0.05, ***p<0.001 between

indicated groups) AAV-Nrg1-I was injected in the gastrocnemius muscle of wild type mice 14 days prior to the injury for ensuring the maximum Nrg1-I expression. (c) The proportion of occupied end plates and of collateral sprouts at 15 days after rhizotomy was similar in AAV-Nrg1-I and vehicle injected muscles, whereas lapatinib injected muscles had lower proportion of innervated endplates (** $p < 0.001$). (d) The percentage of endplates occupied by collateral sprouts and the number of collateral sprouts counted in the gastrocnemius muscle after rhizotomy were similar to control mice in mice injected AAV-Nrg1-I and significantly reduced in lapatinib injected mice (** $p < 0.001$ between indicated groups). (e) Molecular profile after AAV-Nrg1-I and lapatinib administration. Nrg1-I protein was increased in AAV-Nrg1-I injected animals, whereas lapatinib treatment produced a dramatic reduction in the endogenous Nrg1-I and ErbB4 receptor expression, accompanied by an inactivation of Akt and ERK1/2 signaling pathways (One-way ANOVA, ** $p < 0.01$ vs. naive; ## $p < 0.01$ vs. vehicle). For all graphs, values are mean \pm SEM.

Supplementary figure 1. Effect of AAV-GFP injection in SOD1^{G93A} mice. (a) Confocal images showing a high number of muscle fibers transduced by the virus and expressing GFP (scale bar = 100 μ m). Arrows and arrowheads show transfected and not transfected muscle fibers, respectively. Note the high ratio of GFP positive transfected muscles fibers. AAV-GFP injection did not produce any alteration of the functional outcome in SOD1^{G93A} mice, assessed by (b) rotarod performance (values are mean \pm SEM), (c) clinical disease onset, and (d) gastrocnemius muscle compound muscle action potential (CMAP, values are mean \pm SEM).

Fig. 1

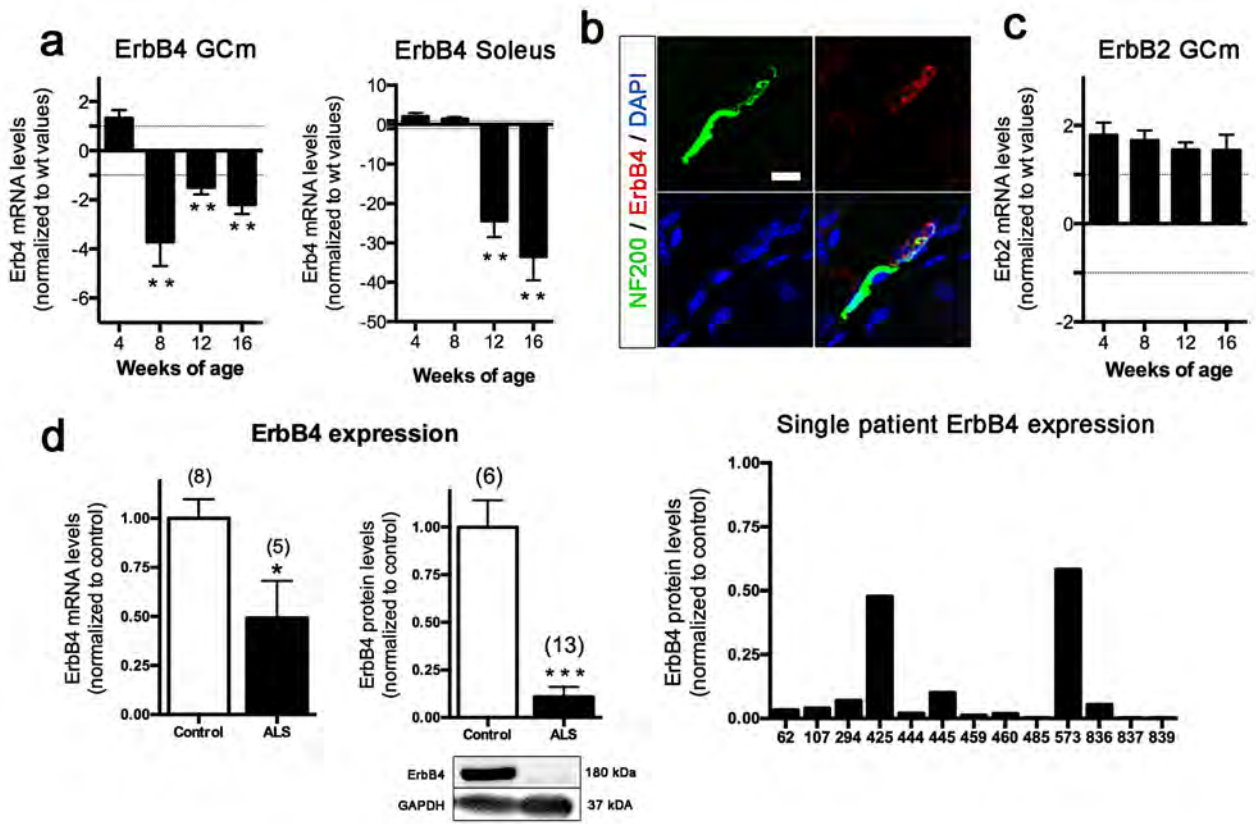


Fig. 2

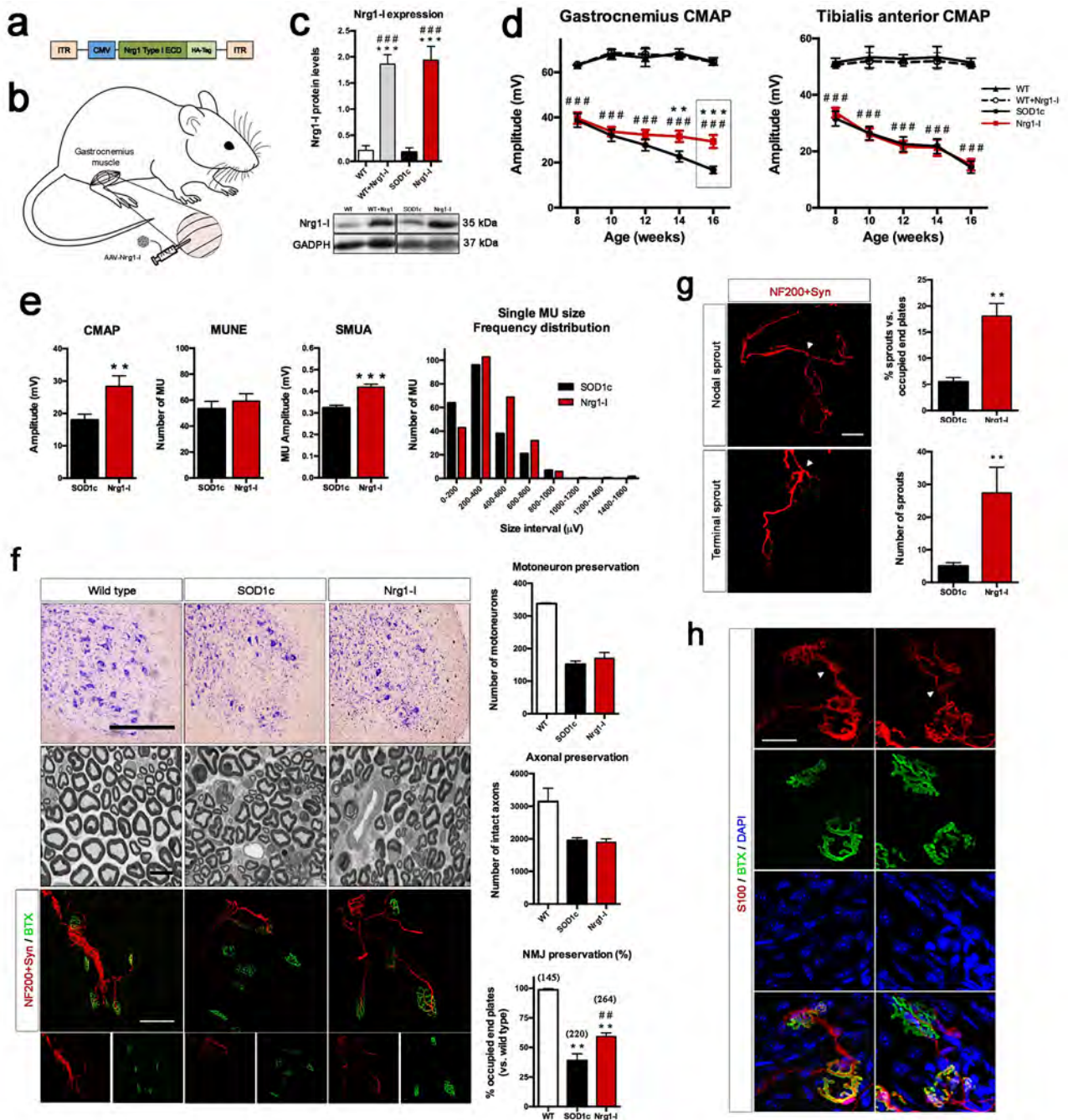


Fig. 3

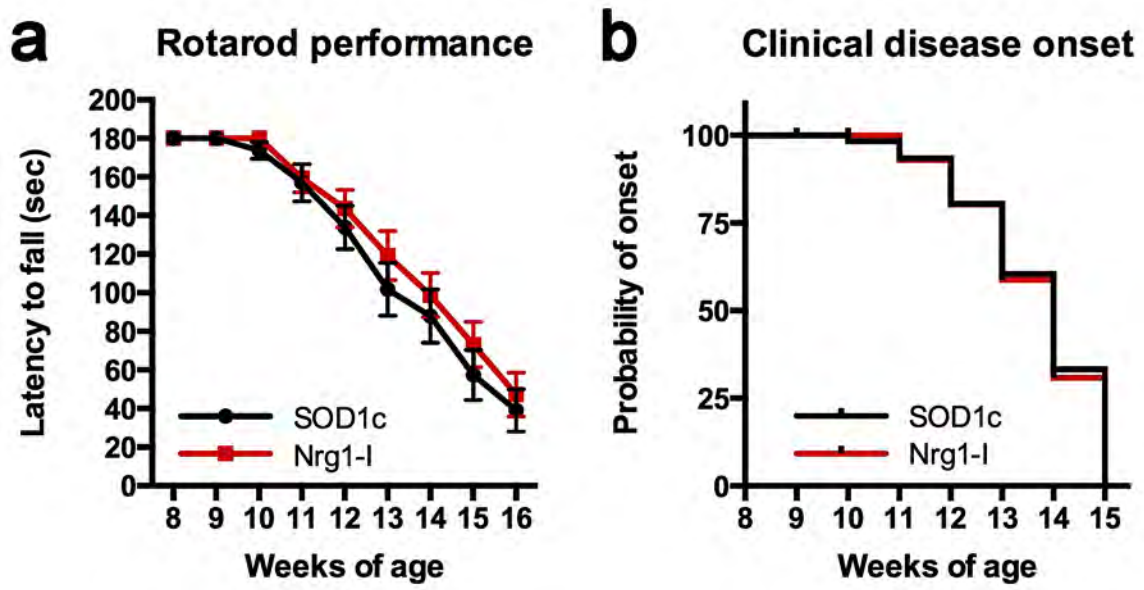


Fig. 4

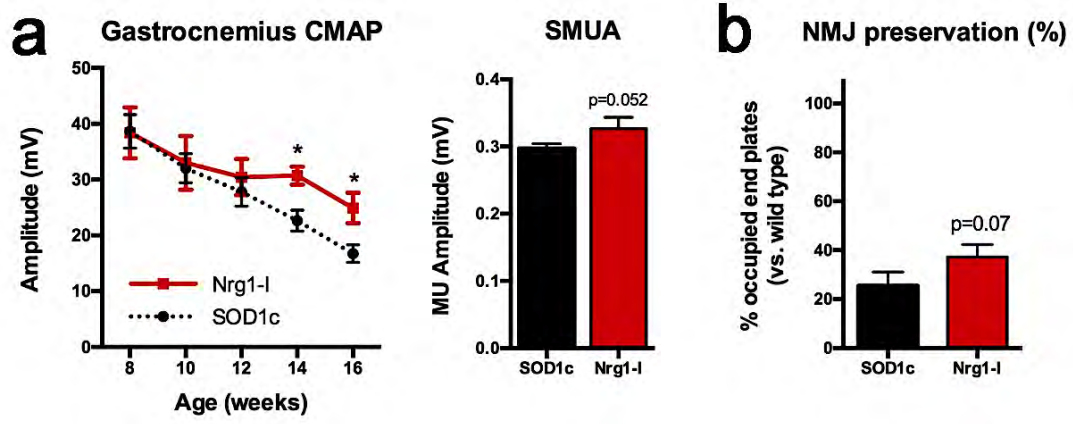


Fig. 5

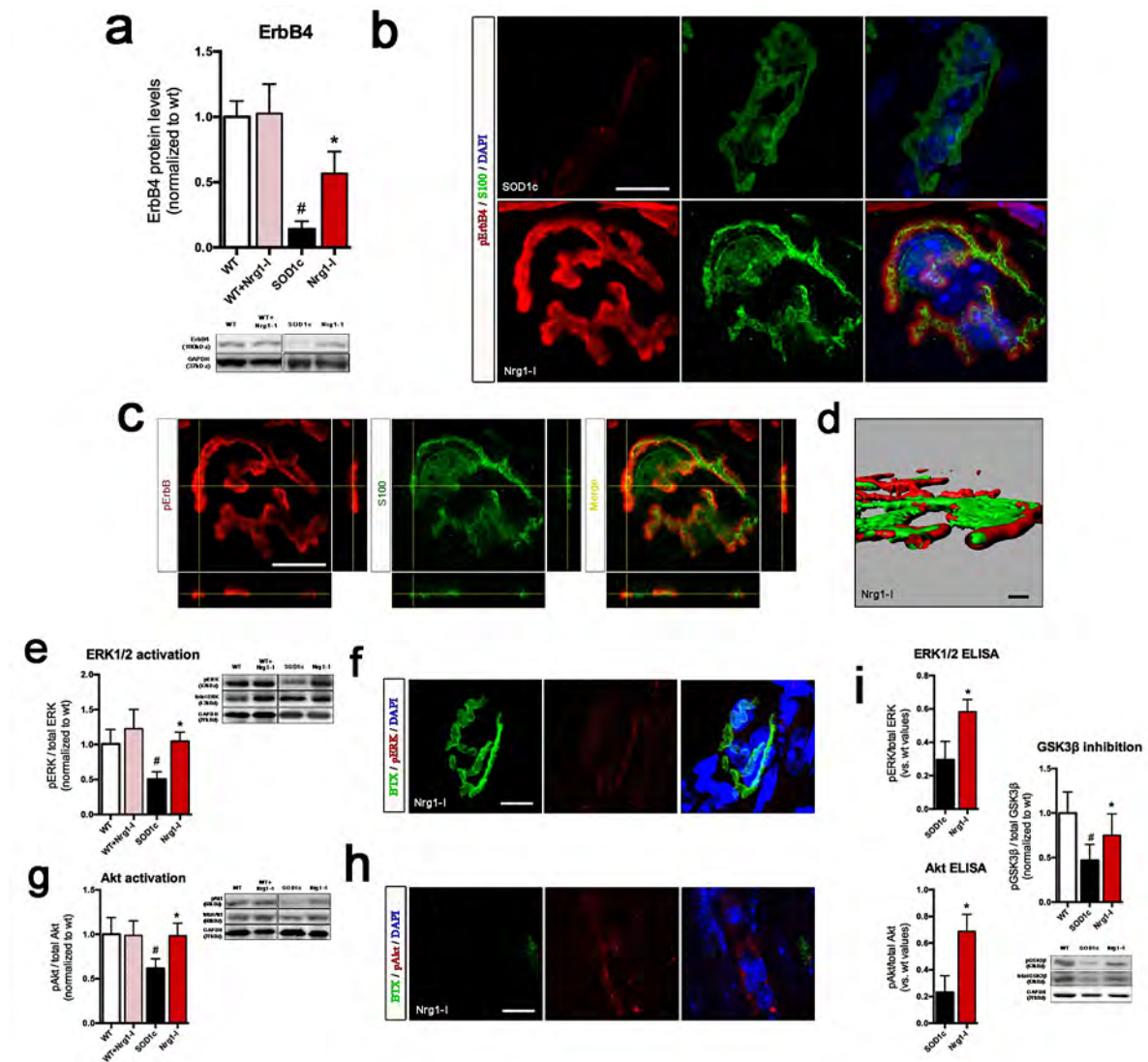


Fig. 6

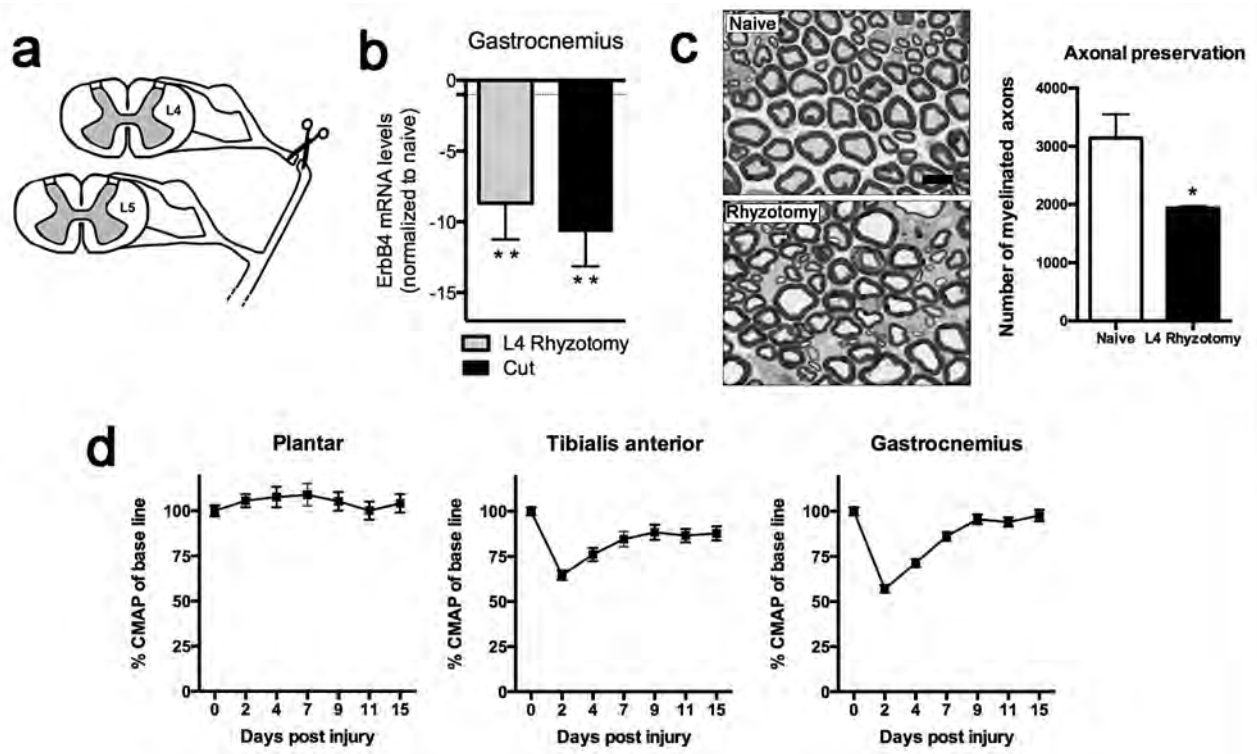
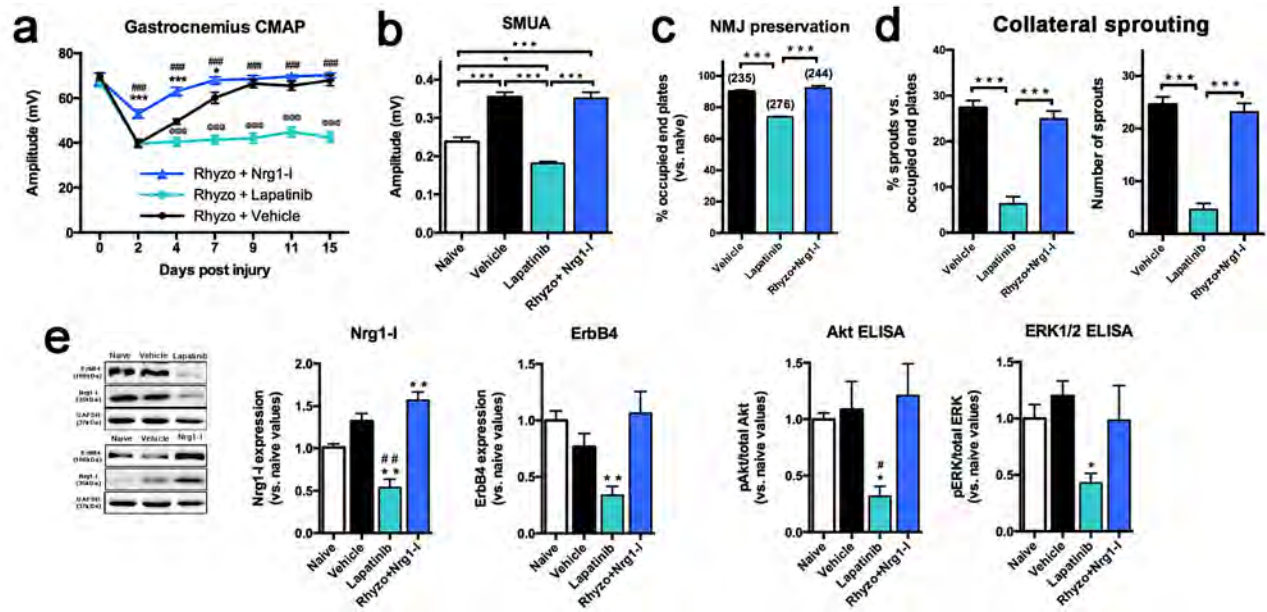


Fig. 7



Supplementary

